Parameterized Logarithmic Framework for Image Enhancement

Karen Panetta, *Fellow, IEEE*, Sos Agaian, *Senior Member, IEEE*,
Yicong Zhou, *Member, IEEE*, and Eric J. Wharton, *Student Member, IEEE*

***Abstract*—Image processing technologies such as image enhancement generally utilize linear arithmetic operations to manipulate images. Recently, Jourlin and Pinoli successfully used the logarithmic image processing (LIP) model for several applications of image processing such as image enhancement and segmentation. In this paper, we introduce a parameterized LIP (PLIP) model that spans both the linear arithmetic and LIP operations and all scenarios in between within a single unified model. We also introduce both frequency- and spatial-domain PLIP-based image enhancement methods, including the PLIP Lee's algorithm, PLIP bihistogram equalization, and the PLIP alpha rooting. Computer simulations and comparisons demonstrate that the new PLIP model allows the user to obtain improved enhancement performance by changing only the PLIP parameters, to yield better image fusion results by utilizing the PLIP addition or image multiplication, to represent a larger span of cases than the LIP and linear arithmetic cases by changing parameters, and to utilize and illustrate the logarithmic exponential operation for image fusion and enhancement.**

***Index Terms*—Alpha rooting (AR), histogram equalization (HE), image enhancement, parameterized logarithmic image processing (PLIP).**

I. Introduction

IMAGE processing is the system of mathematically transforming an image, generally to change some characteristics [1]. This includes many applications such as image enhancement, edge detection, object recognition, and noise reduction. Providing digital images with good contrast and detail is required for many important areas such as vision, remote sensing, dynamic scene analysis, autonomous navigation, and biomedical image analysis [2]. Producing visually natural images or modifying an image to better show the visual information contained within the image is a requirement for nearly all vision and image processing methods [3]. Methods for obtaining such images from lower quality images are called image enhancement techniques. Much effort has been spent extracting information from properly enhanced images [4]–[8]. The enhancement task, however, is complicated by the lack of any general unifying theory of image enhancement as well as the lack of an effective quantitative standard of image quality to aid in the design of an image enhancement system.

Conventionally, image processing methods such as image enhancement utilize linear operations to manipulate images. Current research in image enhancement employs traditional linear arithmetic to implement algorithms based on the human visual system [9]; deconvolution methods [10] or neural models [11] attempting to undo image degradations; histogram modification with hue preservation [12] and other histogram modification techniques [13]–[17]; localized gradient and edge information [18]; and transform-domain-based enhancement techniques using Fourier, cosine, and wavelet transforms [19].

Current practice in image processing makes little use of any standardized mathematically rigorous arithmetical structure specifically designed for image manipulation [20]. Using linear image processing results in some side effects. First, when resulting pixel intensities lie outside the image range, defined as $[0, M)$, they are clipped, causing a loss of information. Second, linear operations typically do not yield results consistent with the physical phenomena.

By solving these common problems in an image processing context, Jourlin and Pinoli developed a logarithmic image processing (LIP) model which is a mathematical framework based on abstract linear mathematics [21]–[25]. It is further studied by Deng [26], [27]. The LIP model contains several specific algebraic and functional operations which can be used to manipulate image intensity values in a bounded range. These operations lead to new techniques to process images more accurately. They generally make use of the logarithm, as transmitted images combine by logarithmic laws and the human visual system processes light logarithmically.

The LIP model has been shown to satisfy Weber's Law and the saturation characteristics of the human visual system [27]–[31]. From a physical point of view, this LIP model is physically justified in a number of aspects. For example, the addition operation is consistent with the transmittance image formation model and the saturation characteristic of the human eye, the contrast definition based on subtraction is consistent with Weber's law, and the zero gray-tone function corresponds to the highest intensity of an image. Additionally, the LIP addition is edge preserving in the context of just noticeable difference [31].

The LIP model has been successfully used for image enhancement [25]–[27], edge detection [24], [32], [33], image filtering [34], and restoration and segmentation [23], [29], [35], [36]. It also has the capability of enhancing color and medical images [37] and performing the convolution operation [38].

Manuscript received September 4, 2009; revised January 7, 2010 and April 29, 2010; accepted July 2, 2010. Date of current version March 16, 2011. This work was supported in part by the National Science Foundation under Grant HRD-0932339. This paper was recommended by Associate Editor P. S. Sastry.

K. Panetta, Y. Zhou, and E. J. Wharton are with the Department of Electrical and Computer Engineering, Tufts University, Medford, MA 02155 USA (e-mail: karen@ece.tufts.edu; yzhou0a@ece.tufts.edu; ewhart02@ece.tufts.edu).

S. Agaian is with the Department of Electrical and Computer Engineering, University of Texas at San Antonio, San Antonio, TX 78249 USA (e-mail: Sos.Agaian@utsa.edu).

Color versions of one or more of the figures in this paper are available online at http://ieeexplore.ieee.org.

Digital Object Identifier 10.1109/TSMCB.2010.2058847

In this paper, we introduce a new parameterized LIP (PLIP) model which includes LIP and linear arithmetic models as special instances and also spans all the cases in between in a single unified model. The new PLIP model will be shown to have the capability of providing better image fusion and enhancement performance than the LIP and linear arithmetic models.

The outline of this paper is as follows. Section II introduces the new PLIP model and discusses its properties. Section III presents the measure of enhancement by entropy (EMEE) which will be used to quantitatively evaluate the performance of the new PLIP model and image enhancement. Section IV presents image fusion using different operations to show the performance of the PLIP model in image manipulation. Section V introduces three new enhancement algorithms using the new PLIP model. Section VI provides representative results of several experiments used to determine the best values of the coefficients. Section VII shows comparative results demonstrating the improved performance of several new PLIP-based enhancement algorithms. Section VIII is a discussion of results, and some concluding comments are made.

TABLE I
SUMMARY OF THE LIP AND PLIP ARITHMETIC OPERATIONS

Traditional LIP	PLIP
$g(i,j) = M - f(i,j)$	$g(i,j) = \mu(M) - f(i,j)$
$g_1 \mathbin{\underset{+}{\triangle}} g_2 = g_1 + g_2 - \frac{g_1 g_2}{M}$	$g_1 \mathbin{\widetilde{\oplus}} g_2 = g_1 + g_2 - \frac{g_1 g_2}{\gamma(M)}$
$g_1 \mathbin{\underset{-}{\triangle}} g_2 = M \frac{g_1 - g_2}{M - g_2}$	$g_1 \mathbin{\widetilde{\Theta}} g_2 = k(M) \frac{g_1 - g_2}{k(M) - g_2}$
$c \mathbin{\underset{\times}{\triangle}} g = M - M\left(1 - \frac{g}{M}\right)^c$	$c \mathbin{\widetilde{\otimes}} g = \gamma(M) - \gamma(M)\left(1 - \frac{g}{\gamma(M)}\right)^c$
$g_1 * g_2 = \varphi^{-1}(\varphi(g_1) \cdot \varphi(g_2))$	$g_1 \mathbin{\widetilde{*}} g_2 = \widetilde{\varphi}^{-1}(\widetilde{\varphi}(g_1) \cdot \widetilde{\varphi}(g_2))$
$\varphi(g) = -M \ln(1 - \frac{g}{M})$	$\widetilde{\varphi}(g) = -\lambda(M) \ln^{\beta}(1 - \frac{g}{\lambda(M)})$
$\varphi^{-1}(g) = M[1 - exp(\frac{-g}{M})]$	$\widetilde{\varphi}^{-1}(g) = \lambda(M)[1 - exp(\frac{-g}{\lambda(M)})^{1/\beta}]$

$f(i,j)$ is the original image intensity, $g(i,j)$, g_1 and g_2 are the gray tone functions, c, β, $(c, \beta > 0)$as a real constant; the new parameters $\mu(M)$, $\gamma(M)$, $k(M)$, $\lambda(M)$ are functions of M that can be trained for the system. $\underset{+}{\triangle}$, $\underset{-}{\triangle}$, $\underset{\times}{\triangle}$ and * stand for LIP addition, subtraction, scalar multiplication, and multiplication of two images, respectively; $\widetilde{\oplus}$, $\widetilde{\Theta}$, $\widetilde{\otimes}$ and $\widetilde{*}$ are the PLIP addition, subtraction, scalar multiplication, and multiplication of two images, respectively.

II. PLIP

In this section, we introduce a new PLIP model by extending the innovative concept of the traditional LIP model introduced by Jourlin and Pinoli [21]. We address the properties of the new PLIP model and some further discussions.

A. PLIP Operations

The traditional LIP model replaces the linear arithmetic operations (addition, subtraction, and multiplication) with nonlinear operations, which more accurately characterizes the nonlinearity of computer image arithmetic. This LIP model is based on gray-tone functions $g(i,j)$ which model light absorption filters. A uniform light source is shone through a filter, and the intensity image is projected onto a screen. In addition, two filters are placed in series. For subtraction, filters are removed, and so forth. The LIP operations shown in Table I model these interactions [22], [26].

A PLIP is presented here. The arithmetic operations make use of a parameterized gray-tone function $g(i,j)$. The PLIP operations are shown in Table I.

The $\mu(M)$ value used to calculate the gray-tone function could be image dependent, such as the maximum value of the image, or it could be some greater value, such as $\mu(M) = 1026$. For simplicity, we use the linear case of $\mu(M) = aM + b$, where a and b are constants to be determined experimentally.

While $\gamma(M)$, $k(M)$, and $\lambda(M)$ can be any functions as a general form, here, we provide the most straightforward case. For other purposes, these could be more complicated functions. It is also noted that addition and scalar multiplication use the same function $\gamma(M)$. This is because scalar multiplication is an extension of addition, adding the image to itself c times.

In addition, we propose an exponential coefficient β to the fundamental isomorphism function $\widetilde{\varphi}$ used for multiplication. In the traditional LIP model, φ is the fundamental isomorphism and converts the gray-tone function to optical light density [21], [23], [25]. By adding this exponential coefficient β, we can fine-tune the multiplication and adjust the sensitivity to either the dark end of the pixel intensity range (small β) or the bright end of the pixel intensity range of $[0, M)$ (large β). This better models the varying response of the human eye at high light intensity versus low light intensity [39] and allows a multiplicative combination without going to saturation. The best value of β is chosen by performing PLIP-based enhancement algorithms or PLIP image multiplication with varying β and assessing the resulting images using the measure of image enhancement.

Since practical applications require exponential operators, which are simply the value multiplied by itself many times, we use the PLIP isomorphic transform and inverse isomorphic transform to denote the PLIP exponential operation

$$g_1^2 = g_1 \mathbin{\widetilde{*}} g_1 = \widetilde{\varphi}^{-1}\left(\widetilde{\varphi}(g_1) \bullet \widetilde{\varphi}(g_1)\right) = \widetilde{\varphi}^{-1}\left(\widetilde{\varphi}(g_1)^2\right). \quad (1)$$

As the associative property holds for grayscale multiplication, it can be shown that a similar derivation works for the cube of a number as well

$$\begin{aligned} g_1^3 &= g_1 \mathbin{\widetilde{*}} g_1 \mathbin{\widetilde{*}} g_1 = g_1 \mathbin{\widetilde{*}} \widetilde{\varphi}^{-1}\left(\widetilde{\varphi}(g_1)^2\right) \\ &= \widetilde{\varphi}^{-1}\left(\widetilde{\varphi}(g_1) \bullet \widetilde{\varphi}\left(\widetilde{\varphi}^{-1}\left(\widetilde{\varphi}(g_1)^2\right)\right)\right) \\ &= \widetilde{\varphi}^{-1}\left(\widetilde{\varphi}(g_1) \bullet \widetilde{\varphi}(g_1)^2\right) = \widetilde{\varphi}^{-1}\left(\widetilde{\varphi}(g_1)^3\right). \end{aligned} \quad (2)$$

This is extended to the general case, giving PLIP exponential, which will be used in Section V for the PLIP alpha rooting (AR) algorithm

$$g_1^n = \widetilde{\varphi}^{-1}\left(\widetilde{\varphi}(g_1)^n\right) \quad (3)$$

where n is a positive integer.

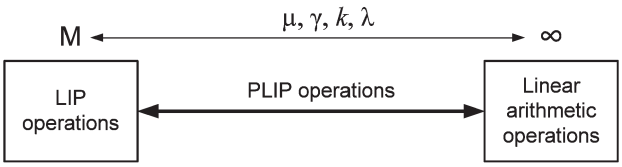

Fig. 1. PLIP operations.

B. Properties of the PLIP Models

1) In the PLIP model, linear arithmetic operations are replaced with new operations in the same manner as the traditional LIP model [37], [40].
2) The PLIP operations revert to the traditional LIP cases when $\mu(M) = \gamma(M) = k(M) = \lambda(M) = M$ and $\beta = 1$.
3) The PLIP operations revert to linear arithmetic operations when $\gamma(M)$, $k(M)$, and $\lambda(M)$ approach the infinity and $\beta = 1$. (The mathematic proofs of this property can be found in Appendix A.)
4) The PLIP operations can generate more cases between the two extreme cases of the LIP and the linear arithmetic operations when the parameters μ, γ, k, and λ change within $[M, \infty)$, as shown in Fig. 1.
5) The output ranges of the PLIP operations. (Mathematical analysis can be found in Appendix B.)
   a) If the pixel intensity range of the input image $f(i,j)$ is $[0, M)$, the range of the PLIP gray-tone function $g(i,j)$ is $(\mu(M) - M, \mu(M)]$. It will be the same as the LIP range $(0, M]$ when $\mu(M) = M$.
   b) If the input gray tone is in the range $(0, \gamma(M)]$, the range of the PLIP addition and scalar multiplication will be $(0, \gamma(M)]$.
   c) If the input gray tone is within $(0, k(M)]$, the range of the PLIP subtraction will be $(-\infty, k(M)]$.
6) It can be shown that PLIP operations obey the laws of associativity, commutativity, a unit element, and distributive properties.
7) The new operations satisfy Jourlin and Pinoli's four fundamental requirements of an image processing framework [28]–[30] in addition to a fifth requirement we have introduced. The following are the requirements.
   a) The framework must be based on a physically relevant image formation model.
   b) The mathematical operations must be consistent with the physical nature of images.
   c) The operations must be computationally effective.
   d) It must be practically fruitful.
   e) It must minimize loss of information.

This fifth requirement is essentially stating that the model must not damage either signal. In essence, when a visually "good" image is added to another visually "good" image, the result must also be "good." This is of particular importance, for example, when receiving information from two sensors which must be somehow fused together.

C. Discussion

LIP operations model light absorption filters. By introducing several parameters, PLIP extends this LIP concept and offers users flexibility to design more specific light filters by changing parameters. Furthermore, more coefficients offer the new PLIP model more robust characteristics to meet more specific and complex requirements in different applications.

Although the strong performance of the LIP models with regard to the human visual system has been shown, there still remains a wide range of tasks which the human visual system can perform effortlessly, while complex algorithms are unable to match this performance. While Weber's and Fechner's laws govern the human visual system for a general case, there is tremendous variability in the human visual system, and for individuals, there are variabilities between different people and between any different imaging sensors.

Parameterizing using the PLIP model allows for this "personalization." In the following section, we will discuss how the PLIP model can solve some challenging issues in image fusion.

III. EMEE

To designate a result as most favorable, it is necessary to establish some objective criteria for quantifying results [41]. Automatic image enhancement based on human visual requirements remains a very challenging problem. There is no single method of image enhancement method that works well for all images [42]. This problem becomes more pressing when one needs to enhance thousands of images in an automated setting.

The EMEE has been proven as an effective measure for evaluating image enhancement quality [41]. This measure is based on the same psychovisual laws which form the basis of the LIP and PLIP models. Therefore, it establishes an *a priori* link between the two [41]–[43]. This makes the EMEE effective for training as a cost function.

The EMEE is calculated by dividing an image $I(i,j)$ into $k_1 \times k_2$ blocks, obtaining the local maximum $(I_{\max k,l})$ and minimum $(I_{\min k,l})$ within each block individually, then processing them using the following equation [43]:

$$EMEE_{\alpha,k_1,k_2} = \frac{1}{k_1 k_2} \sum_{l=1}^{k_1} \sum_{k=1}^{k_2} \left[\alpha \left(\frac{I_{\max k,l}}{I_{\min k,l}} \right)^{\alpha} \ln \left(\frac{I_{\max k,l}}{I_{\min k,l}} \right) \right] \quad (4)$$

where α is a constant which can help to select parameters. We choose $\alpha = 1$ and the block size 4×4 for calculating the EMEE results in this paper.

IV. Image Fusion Using PLIP

Image enhancement systems rely on performance of their basic arithmetical components. We study these most basic building blocks for improved performance.

Since addition is a form of fusion, it is a natural requirement to combine images in a more meaningful fashion. Ideally, added images will be representative of the originals without unnaturally becoming too dark or too bright. In general, the procedures of the LIP and PLIP additions are the same. The original images first are converted into gray-tone images and then performed by the addition operation. The added images are transformed back into grayscale images using the same gray-tone function.

Fig. 2 shows the need for training. It is the combination of an image of a tank with an image of several rocks, where the resulting image should appear to have the tank navigating

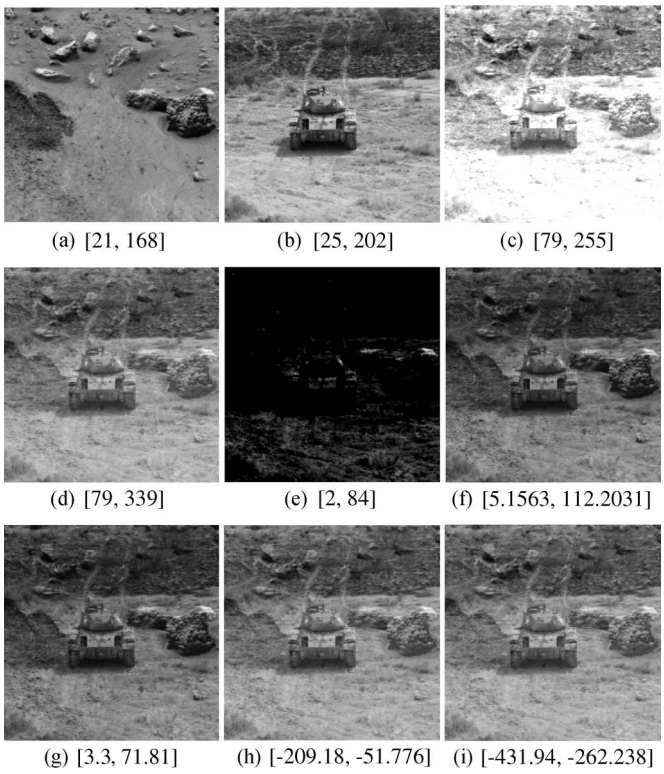

Fig. 2. Fusion of two grayscale images using different image formats and different addition operators, with the minimum and maximum pixel intensity values shown in brackets. (a) Original rock image. (b) Original tank image. (c) Linear addition of two images both in uint8 format. (d) Linear addition of two images both in double format. (e) LIP addition of images of two images both in uint8 format ($M = 256$). (f) LIP addition of two images both in double format ($M = 256$). (g) PLIP addition of two images both in double format ($\mu(M) = \gamma(M) = 400$). (h) PLIP addition of two images both in double format ($\mu(M) = 500$ and $\gamma(M) = 1000$). (i) PLIP addition of two images both in double format ($\mu(M) = 800$ and $\gamma(M) = 2000$).

through the rocks. The pixel intensity ranges for each image are shown at the bottom of the images. For example, [21, 168] in Fig. 2(a) means that the minimum and maximum values of the image are 21 and 168, respectively.

For original images in uint8 format, the resulting images of their linear arithmetic addition are always brighter than the originals. This can make images too bright as shown in Fig. 2(c). However, the resulting images of the LIP addition are always darker than the originals. This makes images generally too dark as shown in Fig. 2(e). This is because many of the pixel intensity values are outside the grayscale range [0, 255]. The pixel values are simply set to 255 for those greater than 255 and to zero for those less than zero. This results in a loss of information.

If the original images are in double format, the results of the linear and LIP additions show better visual quality than those in uint8 format as shown in Fig. 2(d) and (f). Therefore, we use only the double image format for computer simulation in the rest of this paper.

The LIP model maintains the values in the range, and the output is more representative. The result of the linear addition is slightly brighter as shown in Fig. 2(d). The result of the LIP addition looks somewhat darker than originals as shown in Fig. 2(f). This also demonstrates the limitation of LIP arithmetic wherein some output images can be visually damaged. The resulting images are dark and need to be improved.

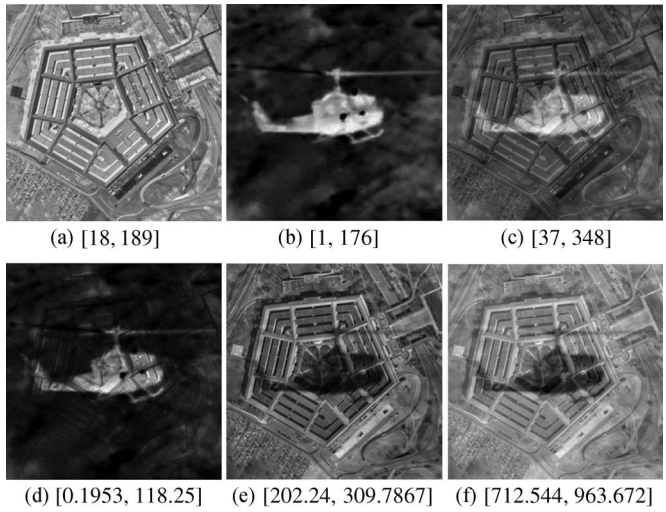

Fig. 3. Fusion of two gray-tone images using LIP and PLIP additions. The minimum and maximum pixel intensity values are shown in brackets. (a) Gray-tone image of the Pentagon image using the LIP equation $g(i, j)$ with $M = 256$. (b) Gray-tone image of Copter image using the LIP equation $g(i, j)$ with $M = 256$. (c) Linear addition. (d) LIP addition ($M = 256$). (e) PLIP addition ($\mu(M) = 500$ and $\gamma(M) = 300$). (f) PLIP addition ($\mu(M) = 1000$ and $\gamma(M) = 500$).

The PLIP model addresses these issues as shown in Fig. 2(g)–(i). These results are visually pleasing and representative images with the selection of appropriate PLIP parameters. The effects of changing $\mu(M)$ and $\gamma(M)$ can allow for better contrast enhancement.

Fig. 3 shows one of the advantages of the PLIP model. The pixel intensity ranges for all images are also shown in brackets in the bottom of the corresponding images. The two input images are gray-tone functions of the Pentagon and Copter images, respectively. The linear and LIP additions can result only gray-tone images as shown in Fig. 3(c) and (d). However, the PLIP addition can obtain not only gray-tone images but also the grayscale images by selecting appropriate parameters $\mu(M)$ and $\gamma(M)$. Vice versa, if the input images are grayscale images, the PLIP addition can obtain an added image with a gray-tone format with specific values for $\mu(M)$ and $\gamma(M)$.

The β parameter gives a greater control over the logarithmic function for the multiplication of two images. It can assign increasing weight to the higher or lower end of the pixel saturation range. Fig. 4 shows that, when the parameter $\lambda(M)$ is negative, the β plays an important role for the PLIP multiplication of two images. The original intensity images first are converted to gray-tone functions, processed by the PLIP image multiplication, and then transformed back into intensity images by the same gray-tone equation in Table I. Fig. 3(c) shows a case of the LIP image multiplication. The resulting image is unrecognizable. This is the same as the case of the PLIP multiplication with $\lambda(M) = 256$ and $\beta = 1$. However, for the cases of negative $\lambda(M)$ as shown in Fig. 4(d)–(f), β values yield visually appealing images. This is another advantage of the PLIP model.

V. New PLIP-Based Image Enhancement Algorithms

The goal of image enhancement techniques is to improve the characteristic or quality of an image, such that the resulting

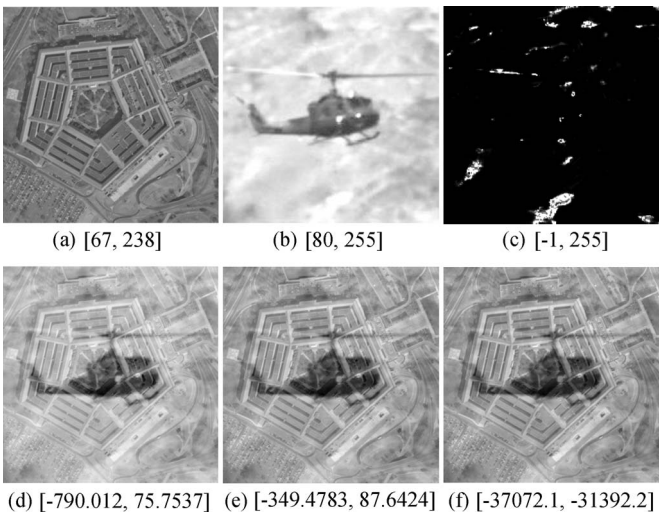

Fig. 4. Testing the optimal β using the PLIP image multiplication. (a) Original Pentagon image. (b) Original Copter image. (c) Traditional LIP image multiplication ($\beta = 1$). (d) PLIP image multiplication ($\mu(M) = 500$, $\lambda(M) = -500$, and $\beta = 5$). (e) PLIP image multiplication ($\mu(M) = 1026$, $\lambda(M) = -1026$, and $\beta = 10$). (f) PLIP image multiplication ($\mu(M) = 4100$, $\lambda(M) = -1000$, and $\beta = 19$). This shows that β plays an important role for PLIP image multiplication when $\lambda(M)$ is negative.

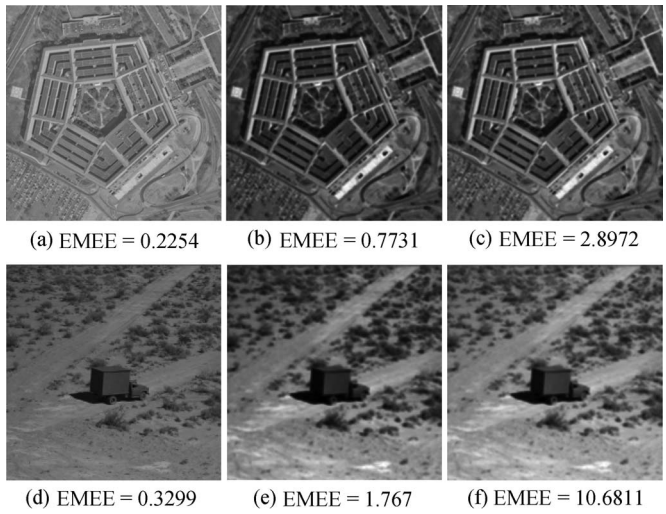

Fig. 5. Comparison of PLIP LA with LIP LA. (a) Original image. (b) Image enhanced by LIP LA ($M = 256$, $\eta = 0.5$, $\sigma = 100$, and $\delta = 0.15$). (c) Image processed with PLIP LA ($\mu(M) = \gamma(M) = k(M) = \lambda(M) = 500$, $\eta = 0.42$, $\sigma = 450$, and $\delta = 0.2$). (d) Original image. (e) Image enhanced by LIP LA ($M = 256$, $\eta = 0.4$, $\sigma = 200$, and $\delta = 0.19$). (f) Image processed with PLIP LA ($\mu(M) = \gamma(M) = k(M) = \lambda(M) = 600$, $\eta = 0.4$, $\sigma = 300$, and $\delta = 0.25$).

image is better than the original by some specific criteria [44]. Current research in image enhancement covers such wide topics as algorithms for color correction [45]–[47], JPEG-based enhancement for the visually impaired [48], and histogram modification techniques [12], [13], [43], [49].

In [50], the authors state that the main challenge remains in the following application areas: development of high-quality image enhancement methods that do not destroy the color code information, development of quantitative measures of view ability for such images, and automating the process of image enhancement that meets human expert approval. These issues are addressed in detail in this paper.

There are several commonly used enhancement methods such as Lee's algorithm (LA) [51], bihistogram equalization (BHE) [15], and alpha rooting (AR) [52]. In this section, we present three novel PLIP-based image enhancement algorithms, namely, PLIP LA, PLIP BHE, and PLIP AR. These are accomplished by simply changing the linear arithmetic with the new PLIP operations and varying the parameters. We will use these algorithms to demonstrate the improved enhancement performance using the PLIP. For simplicity, we choose $\mu(M) = \gamma(M) = k(M) = \lambda(M)$ for computer simulation.

A. PLIP Lee's Algorithm

In 1980, Lee proposed a simple algorithm for image enhancement, which can be expressed as [51]

$$F'(i,j) = \theta A(i,j) + \rho + \zeta\left[F(i,j) - A(i,j)\right] \tag{5}$$

where $F(i,j)$ and $F'(i,j)$ represent the pixel brightness values of the original and processed images; $A(i,j)$ is the arithmetic mean brightness value of an $n \times n$ window that is centered on the pixel position (i,j); and θ, ρ, and ζ are the weight coefficients.

LA first decomposes an image into two parts, a smooth image and a difference image. These images are then weighted and recombined. The algorithm was extended by using the traditional LIP operators for image enhancement [27], [31], [40]. It can be further improved by using PLIP operators, called PLIP LA, which is defined by the following expression:

$$f'(i,j) = \eta \widetilde{\otimes} a(i,j) \widetilde{\oplus} \sigma \widetilde{\oplus} \delta \widetilde{\otimes} \left[f(i,j) \widetilde{\Theta} a(i,j) \right] \tag{6}$$

where $f'(i,j)$ is the output gray-tone function; $f(i,j)$ is the input gray-tone function; $a(i,j)$ is the PLIP average of the pixels surrounding the given pixel; and η, σ, and δ are user-defined operating constants.

To demonstrate the effects of the PLIP LA, we compare enhanced images by using the traditional LIP and PLIP models, as shown in Fig. 5. The PLIP model allows for resulting images to both get brighter and darker appropriately, yielding improved contrast. The enhanced images using traditional LIP in Fig. 5(b) and (e) show improved contrast, but some details are not as clear as they could be. The enhanced images using the PLIP not only have improved contrast but also show all details clearly, as shown in Fig. 5(c) and (f). The EMEE values confirm that the PLIP LA outperforms the LIP LA.

It can also be seen that the proposed PLIP LA is more sensitive to noise than LA. Since noise is generally in the higher frequency components and the PLIP LA combines a high-pass image with a low-pass image, it can emphasize any noise in the image.

B. PLIP BHE

BHE [15] is based on standard histogram equalization (HE). A histogram of a gray image is the discrete distribution function of the gray levels of the pixels. When a photograph is transformed so that all the gray levels occur equally often, the result tends to have a higher contrast [14]. Standard HE uses

a cumulative density function to attempt to force a uniform distribution for the image, according to the following formula:

$$f(x) = X_{\min} + (X_{\max} - X_{\min}) \cdot C(x) \tag{7}$$

where x is the input pixel intensity within the range $[X_{\min}, X_{\max}]$, $f(x)$ is the output pixel intensity, $X_{\min}$ and $X_{\max}$ are the minimum and maximum values for the desired output range, and $C(x)$ is the cumulative distribution function, where $C(X_{\max}) = 1$.

BHE introduces a threshold parameter to better control over the enhancement and to obtain a better image [15]–[17]. It first decomposes an image into two subimages based on a global threshold. These two subimages are enhanced using standard HE separately.

Many BHE-based methods have been developed to preserve brightness by setting the threshold at the mean gray level [15], by selecting the threshold as the median value in an attempt to maximize entropy [16], and by predicting the brightness error as a cost function to select the threshold [17].

To improve the performance of BHE, we introduce a PLIP-based BHE defined by

$$f(x) = \begin{cases} X_{\min} \widetilde{\oplus} C_L(x) \widetilde{\otimes} (X_T \widetilde{\Theta} X_{\min}), & x \le X_T \\ X_T \widetilde{\oplus} C_H(x) \widetilde{\otimes} (X_{\max} \widetilde{\Theta} X_T), & x > X_T \end{cases} \tag{8}$$

where X_T is the threshold for separating the input image into two subimages and $C_L(x)$ and $C_H(x)$ are the cumulative distribution functions of the low and the high subimage, respectively. The PLIP scalar multiplication $\widetilde{\otimes}$ can be replaced by $\widetilde{*}$ for different applications.

Fig. 6 compares BHE with the linear, LIP, and PLIP operations. Fig. 6(a)–(d) shows the linear case. The enhanced result is satisfactory but can be improved upon. Fig. 6(e)–(g) shows the LIP BHE, and Fig. 6(h)–(j) shows the PLIP case. The PLIP enhanced image improves the results using linear and LIP arithmetic. It has a more consistent appearance between the two subimages and better details in the truck and shrubberies. This assessment is reinforced by an improved EMEE score.

To show the improvement of using PLIP BHE, we summarize enhancement results using the EMEE measure. Table II compares resulting EMEE values for a number of images processed by BHE with the LIP and PLIP. For each image, the PLIP BHE yields higher EMEE values compared with the LIP BHE.

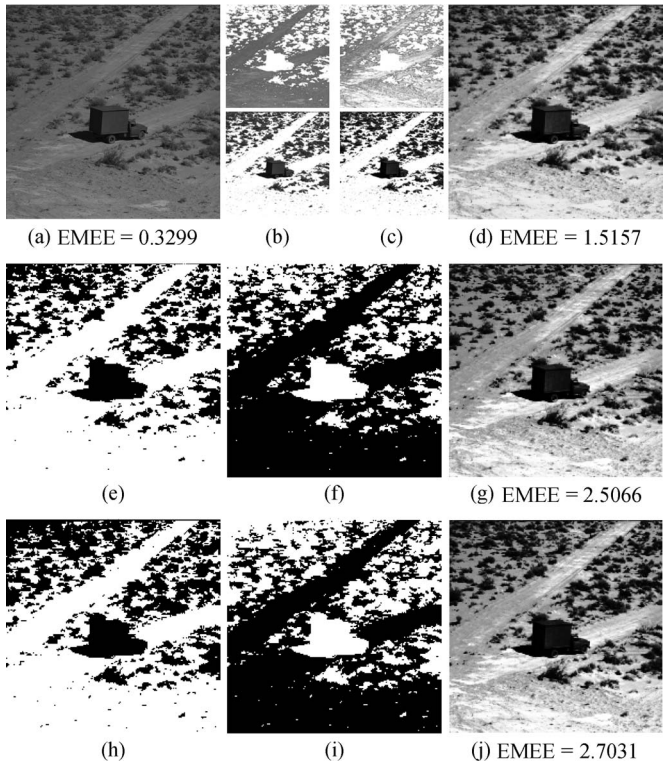

Fig. 6. Comparison of BHE methods with linear and PLIP arithmetic, showing improved performance of the PLIP. (a) Original image. (b) (Top) High subimage and (bottom) low subimage separated from the original image. (c) (Top) High subimage and (bottom) low subimage are enhanced linearly. (d) Linearly enhanced image. (e) Traditional LIP enhanced low subimage. (f) Traditional LIP enhanced high subimage. (g) Traditional LIP enhanced image with *threshold 160* ($M = 256$). (h) PLIP enhanced low subimage. (i) PLIP enhanced high subimage. (j) PLIP enhanced image with *threshold 97* ($\mu(M) = \gamma(M) = k(M) = \lambda(M) = 200$).

TABLE II
COMPARISON EMEE RESULT USING TRADITIONAL LIP BHE TO PLIP BHE

Image	Original Image	LIP	PLIP
Pentagon	0.2254	0.4645	0.6448
Copter	0.0359	0.1088	0.1321
Lena	0.2941	0.4311	0.5535
Plane	0.334	0.9178	1.45
Tank	0.2294	0.4525	0.6764
Arctic Hare	0.012	0.0293	0.0422
Business	0.8941	2.0532	2.576
Plant	0.5343	1.8958	2.0594

Higher EMEE values indicate better enhancement performance.

C. PLIP Alpha Rooting

AR is a straightforward and effective transform enhancement algorithm. AR-based methods have been used for image enhancement such as a preprocessing enhancement stage for edge detection [53], medical image enhancement [54], [55], and enhancement in the JPEG domain for people with visual impairment [48].

AR first transforms the original image into a transform domain by using some orthogonal transform such as the discrete Fourier transform (DFT). It then modifies the magnitude of the transform coefficients, while the phase is kept invariant. The enhanced image is obtained by performing the inverse transform [19], [41], [52], [55]. The magnitude of coefficient is modified by

$$O(p,s) = X(p,s) \times |X(p,s)|^{\alpha - 1} \tag{9}$$

where $O(p,s)$ and $X(p,s)$ are the DFTs of the output and input images, respectively, and $0 < \alpha < 1$.

To demonstrate a new application of the AR for logarithmic models as well as a new application of the PLIP exponential operation for image enhancement in the transform domain, we introduce a new PLIP AR algorithm. It applies PLIP operations, namely, the PLIP exponentiation given in (3) for the AR as defined in (9). The input and output transforms of the

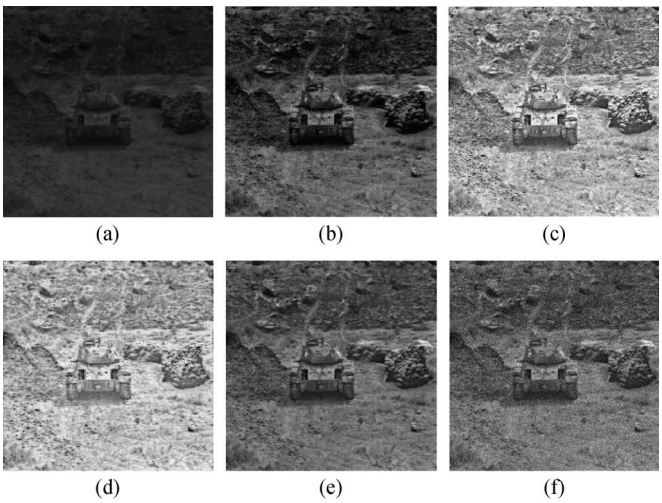

Fig. 7. Comparison of traditional AR, LIP, and PLIP AR by using different parameter values. (a) Original image from Fig. 2(f). (b) Image enhanced by the traditional AR defined in (9) ($\alpha = 0.9$). (c) Image enhanced by the LIP AR ($\alpha = 0.97$). (d) Image enhanced by the PLIP AR ($\mu(M) = \lambda(M) = 800$, $\alpha = 0.98$, and $\beta = 0.45$). (e) Image enhanced by the PLIP AR ($\mu(M) = \lambda(M) = 800$, $\alpha = 0.98$, and $\beta = 1$). (f) Image enhanced by the PLIP AR ($\mu(M) = \lambda(M) = 800$, $\alpha = 0.98$, and $\beta = 1.5$). These show that the image using $\mu(M) = \lambda(M) = 800$ and $\beta = 1$ is the most visually natural, and higher values of β give more enhancement of textures and objects.

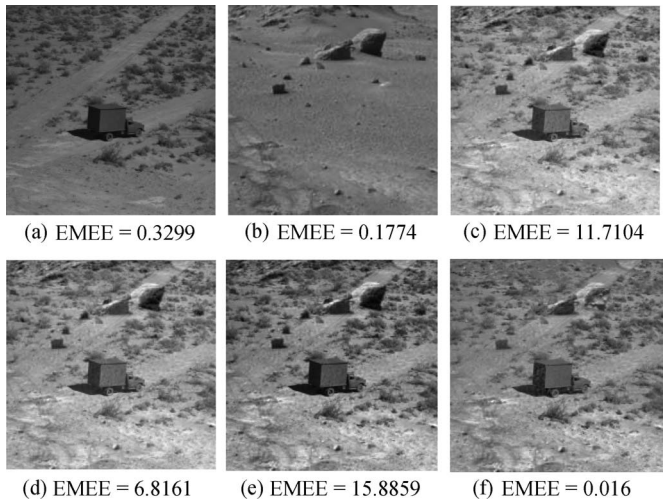

Fig. 8. Effect of changing $\mu(M)$ can be seen while keeping the other parameters the same ($\lambda(M) = 512$). (a) Original image with maximum intensity 169. (b) Original image with maximum intensity 203. (c) Their collective maximum $\mu(M) = 203$. (d) $\mu(M) = 300$. (e) $\mu(M) = 500$. (f) $\mu(M) = 600$.

gray-tone images ($X(p, s)$ and $O(p, s)$) are used. The PLIP AR is defined by

$$O(p,s) = \widetilde{\varphi}^{-1}\left(\widetilde{\varphi}\left(|X(p,s)|\right)^{\alpha-1}\right) \bullet X(p,s) \qquad (10)$$

where $\widetilde{\varphi}(.)$ and $\widetilde{\varphi}^{-1}(.)$ are the PLIP isomorphic transform and PLIP inverse isomorphic transform, respectively.

Fig. 7 shows the new PLIP AR for image enhancement. Fig. 7(a) shows the original image which is generally too dark. Fig. 7(b) shows the result enhanced by traditional AR. The enhanced image shows improved contrast, but it is slightly unnatural. LIP AR obtains an enhanced image with a more visually natural appearance as shown in Fig. 7(c). Fig. 7(d)–(f) shows the results for several values of PLIP parameters. These demonstrate how change of the PLIP parameters affects the enhanced images.

The LIP can be considered as a special PLIP case for $\mu(M) = \lambda(M) = 256$. The effect of $\lambda(M)$ is not great compared to images shown in Fig. 7(c) and (e). There are some minor changes in the overall contrast. Images in Fig. 7(d)–(f) demonstrate that changing the β parameter can result in a major effect on the output image. Changing β forces the users to change the α parameter in (9) appropriately. The enhanced images with lower β are generally more saturated in the overall appearance as shown in Fig. 7(d). However, the larger β shows better performance for enhancing textures and objects as shown in Fig. 7(f).

VI. Methods to Train the PLIP

In this section, we present the training system used to select the best values for the PLIP parameters. This is accomplished by choosing the local extrema from the plot of the EMEE versus the parameters.

The best (optimal) parameter is obtained if the following condition is satisfied:

$$EMEE_{\text{optimal}} = \max_{\text{local}}\left(EMEE(\alpha, \mu, \gamma, k, \lambda, \beta)\right) \qquad (11)$$

where $EMEE_{\text{optimal}}$ is the optimized EMEE value of the enhanced image, $\max_{\text{local}}(X)$ is a function to obtain the local maximum value of X, and $EMEE(\alpha, \mu, \gamma, k, \lambda, \beta)$ is the EMEE measure result when the parameters α, μ, γ, k, λ, and β change.

We use these parameters to obtain the best enhanced images. The results will be verified by the EMEE values and visual assessment.

A. Assessment by EMEE Values

To train the parameters μ, γ, k, and λ, we used two methods. We tested the different atomic operations individually and also tested several enhancement algorithms. We performed these studies using several different values of the PLIP parameters and compared the resulting images.

We first demonstrate the improved performance by training only the $\mu(M)$ value using PLIP addition of two images shown in Fig. 8(a) and (b). $\mu(M)$ is used to calculate the gray-tone functions for two images. The results using the maximum value of the two images collectively and $\mu(M) = 300$ have a similar visual appearance as shown in Fig. 8(c) and (d). The major difference between them is in the background. By using the maximum value of the two images collectively, the background in the truck image is given higher values than that in Fig. 8(d). This helps to hide some of the ripples in the sand as shown in the lower left hand corner of the image. The images in Fig. 8(e) and (f) are more visually appealing images. The image in Fig. 8(e) has a higher EMEE value.

We test the scenario where different operations use different values for the parameters. Many important properties such as inverse operations ($g_1 \widetilde{\oplus} g_2 \widetilde{\Theta} g_2 = g_1$) are important theoretically and practically. They may require that the parameters are

Fig. 9. Demonstration of the case where the parameters are not equal. (a) Original Lena image. (b) Original Pentagon image. (c) Addition of Lena and Pentagon using $\gamma(M) = 1026$. (d) Subtraction of (a) from (c) ($k(M) = 256$). (d) Subtraction of (a) from (c) ($k(M) = 512$). (f) Subtraction of (a) from (c) ($k(M) = 1026$). This shows subtraction using the correct value for $k(M)$.

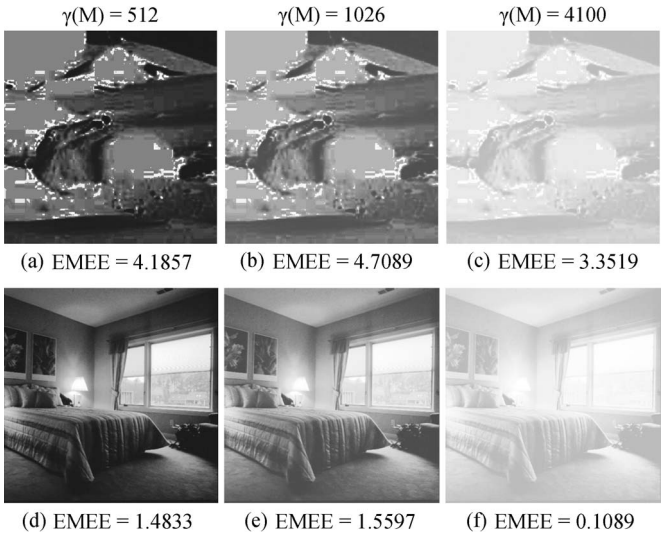

Fig. 10. Effects of changing the parameter are demonstrated using simple images processed with traditional HE. Images (a)-(c) show the Arctic Hare image, and images (d)-(f) show the bed image, processed using HE and with values of the parameters as shown above the images. This shows that even though other values may produce good results, using γ, k, and $\lambda = 1026$ yields good results for the general case.

the same. We test the practical effect of using different values for the parameters.

Fig. 9 shows an example of the most basic operations. An image is added to and subtracted from another image. In Fig. 9, the Pentagon image is added to Lena using $\gamma(M) = 1026$ and then subtracted using various values for $k(M)$. As expected, only the image where $\gamma(M) = k(M)$ matches the original Lena image. In the images with $k(M) < \gamma(M)$, the Pentagon image slowly fades out as $k(M)$ gets closer to $\gamma(M)$. While this is a theoretical issue, it could be used in practical applications such as data hiding.

Other values for these parameters may work well in some cases. Fig. 10 shows that $\gamma = k = \lambda = 1026$ generally yields

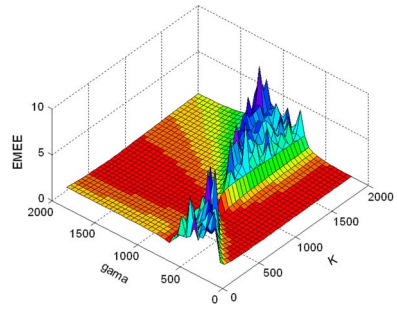

Fig. 11. EMEE versus $\gamma(M)$ versus $k(M)$ for Pentagon image processed by using PLIP BHE (threshold is 140 and $\mu(M) = 1026$). Note that the curve in this figure uses the logarithmic values of EMEE results to show the EMEE peak changes only for the display purpose.

Fig. 12. Testing the optimal $\gamma(M)$ and $k(M)$ values with PLIP BHE. (a) Original Pentagon image. (b) Enhanced image (threshold $= 140$, $\mu(M) = 1026$, $\gamma(M) = 500$, and $k(M) = 500$). (c) Enhanced image (threshold $= 140$, $\mu(M) = 1026$, $\gamma(M) = 500$, and $k(M) = 300$).

visually appealing images. These can be verified by EMEE measure results.

B. EMEE Plot Evaluation

The practical usefulness of differing parameters is tested by using PLIP BHE. Fig. 11 shows that the training of the PLIP can improve the performance of image enhancement. The original images are enhanced by PLIP BHE using different values for parameters $\gamma(M)$ and $k(M)$. This study was performed for many images.

Fig. 11 shows only the results for the Pentagon image. These results use $\mu(M) = 1026$ and a fixed threshold value of 140. In order to highlight the EMEE peak value changes, Fig. 11 shows the logarithmic values of EMEE measure results.

Fig. 12 shows the enhanced images using parameters selected from the EMEE plot in Fig. 11. The better enhanced image is shown in Fig. 12(b). This image has the better contrast and is visually appealing. The EMEE values confirm this.

Fig. 13 shows the effect of the Lena image using different values for the parameters. The threshold value is fixed to 140. We attempt to obtain better enhanced images by changing only the PLIP parameter $\gamma(M)$. In the first example, Fig. 13(a)–(c) shows the results using a fixed value of $k(M) = 800$. The resulting image using $\gamma(M) = k(M) = 800$ is too dark. However, when the peak at $\gamma(M) = 1280$ on the EMEE curve in Fig. 13(c) is selected, the resulting image shows improved contrast as shown in Fig. 13(b).

The second example shown in Fig. 13(d)–(f) shows a similar case using $k(M) = 500$. When the parameters are the same ($\gamma(M) = k(M) = 500$), the output image shown in Fig. 13(d) is too bright. When the measure in Fig. 13(f) is used to select

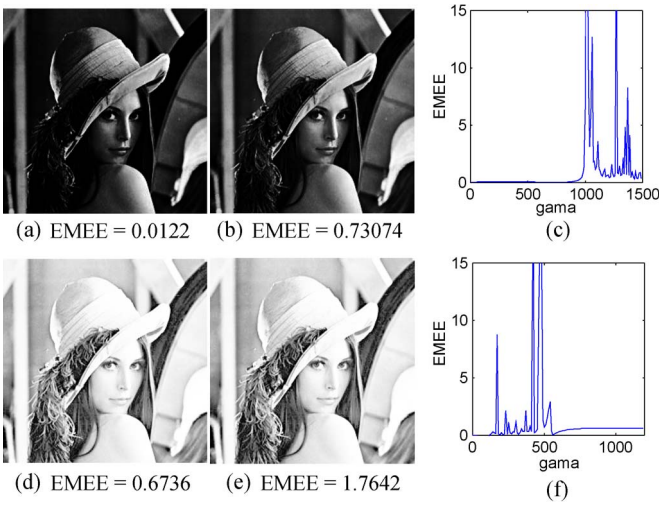

Fig. 13. Practical effect of using different PLIP parameters while maintaining fixed enhancement parameters. (a) and (d) show enhancement results using equal PLIP parameter values. (a) Enhanced image ($k(M) = \gamma(M) = 800$). (b) Enhanced image using $k(M) = 800$ and $\gamma(M) = 1280$. (d) Enhanced image ($k(M) = \gamma(M) = 500$). (e) Enhanced image using $k(M) = 500$ and $\gamma(M) = 526$. (b) and (e) show improved enhancement results when the $\gamma(M)$ parameter is tuned independently of $k(M)$ using the measure in (c) and (f).

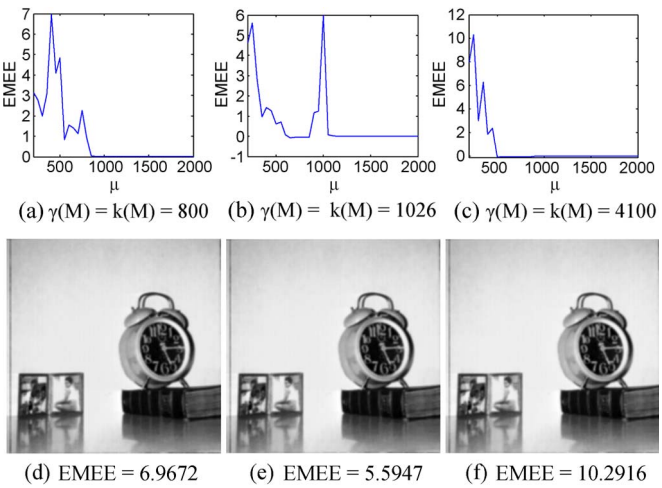

Fig. 14. Testing the optimal $\mu(M)$ values for image enhancement using PLIP LA. (a) EMEE plot ($\gamma(M) = k(M) = 800$). (b) EMEE plot ($\gamma(M) = k(M) = 1026$). (c) EMEE plot ($\gamma(M) = k(M) = 4100$). (d) Enhanced image ($\mu(M) = 400$). (e) Enhanced image ($\mu(M) = 250$). (f) Enhanced image ($\mu(M) = 250$). This shows that $\gamma(M) = k(M) = 4100$ and $\mu = 250$ provide the most visually appealing image.

the $\gamma(M)$ parameter, $\gamma(M) = 526$ can yield an output image with improved contrast. However, from a practical standpoint, the user can obtain more visually pleasing enhanced images by modifying these parameters separately.

Fig. 14 shows the enhanced images by training $\mu(M)$ using EMEE plots for PLIP LA. Fig. 14(a)–(c) shows the EMEE plots using $\gamma(M) = k(M) = 800$, $\gamma(M) = k(M) = 1026$, and $\gamma(M) = k(M) = 4100$, respectively. The enhanced clock images shown Fig. 14(d)–(f) are obtained by using parameters selected from these plots. The enhanced image in Fig. 14(f) shows the better visually appealing and better EMEE measure value than other two.

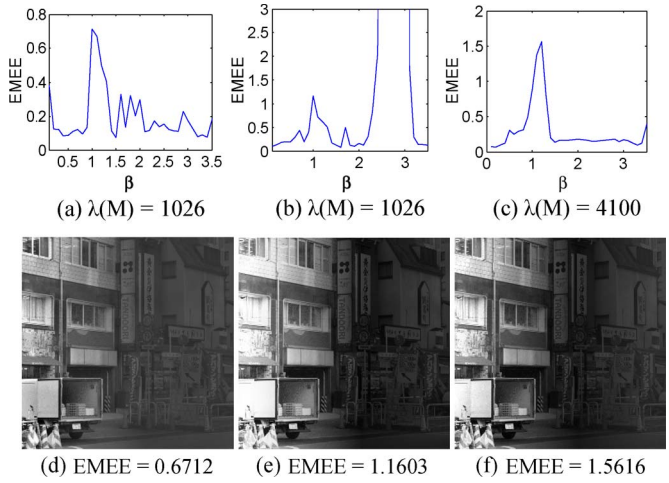

Fig. 15. Testing the optimal β and $\lambda(M)$ values for image enhancement using PLIP AR. (a) EMEE plot ($\lambda(M) = 256$). (b) EMEE plot ($\lambda(M) = 1026$). (c) EMEE plot ($\lambda(M) = 4100$). (d) Enhanced image ($\beta = 1.1$). (e) Enhanced image ($\beta = 1$). (f) Enhanced image ($\beta = 1.2$). This shows that $\lambda(M) = 4100$ and $\beta = 1.2$ provide the most visually appealing image.

The parameter β has control over the PLIP isomorphic transform and its inverse transform used for the PLIP image multiplication. We train this parameter using the EMEE plot. The PLIP AR algorithm is used to enhance images by changing values of β and parameter $\lambda(M)$. Fig. 15 shows the EMEE plot to train the parameters β and $\lambda(M)$. The best operating parameters are chosen by using the EMEE measure. The enhancement algorithm is run for different values of β. The EMEE values and visual inspection of the enhanced results show that parameters $\beta = 1.2$ and $\lambda(M) = 4100$ yield a more visually pleasing enhanced image with better contrast as shown in Fig. 15(f).

VII. Enhancement Comparisons

In this section, we compare the presented PLIP-based enhancement algorithms with several enhancement algorithms with linear and LIP operations. This is to demonstrate how the PLIP operations improve the enhancement performance. We have shown that several possible values and combinations of parameters can improve enhancement performance. For simplicity, however, we choose $\mu(M) = \gamma(M) = k(M) = \lambda(M) = 1026$ for computer simulations.

A. Comparative Results

Fig. 16 shows the original images used for this study. The pentagon, copter, Lena, plane, tank, and arctic hare images are commonly used images. The bed image is a professionally captured image with nonuniform illumination. The business image is a professionally captured image with noise added. The truck and plant images are aerials with atmospheric noise and low definition. Cave and rocks are two images captured by a cell phone with a digital camera.

To show the enhancement performance of the presented PLIP-based algorithms, all 12 images in Fig. 16 are processed by the HE, LA, AR, LIP LA, LIP BHE, PLIP LA, PLIP AR, and PLIP BHE.

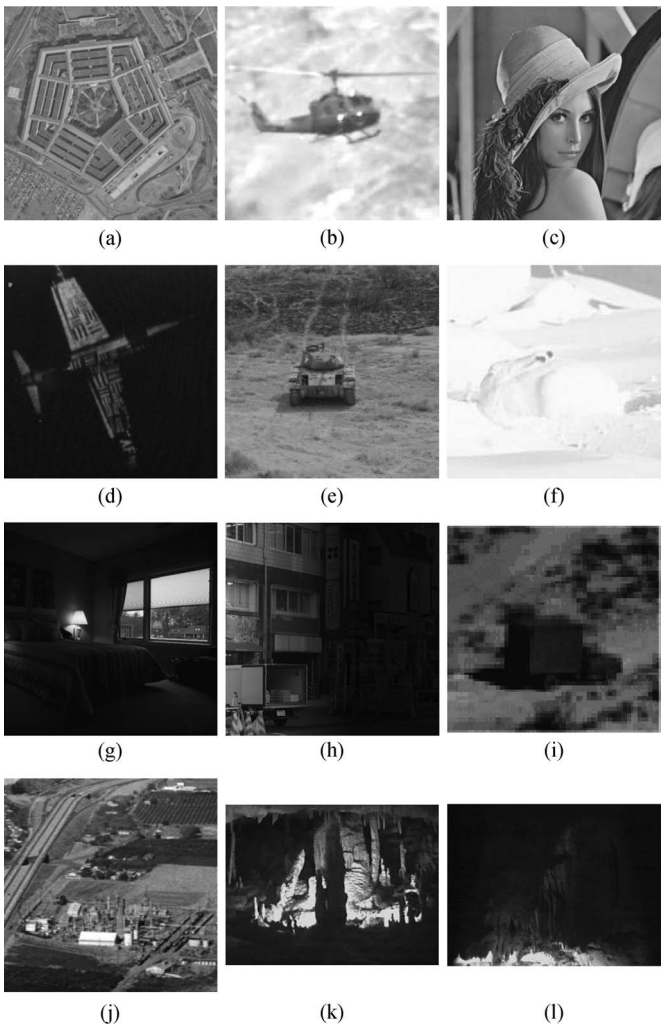

Fig. 16. Original images used to test the proposed methods. (a) Pentagon. (b) Copter. (c) Lena. (d) Plane. (e) Tank. (f) Arctic hare. (g) Bed. (h) Business. (i) Truck. (j) Plant. (k) Cave. (l) Rocks.

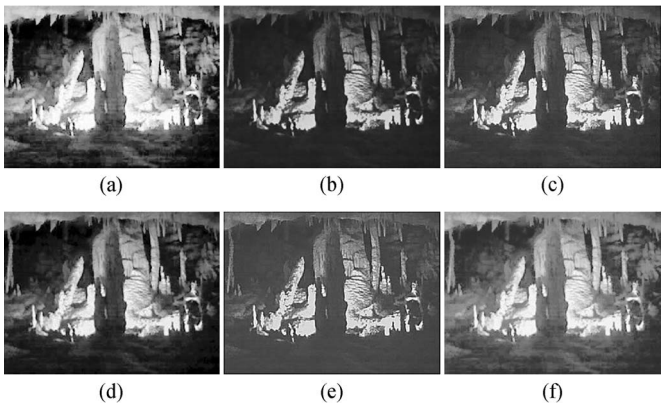

Fig. 17. Comparison of results for the cave image enhanced using (a) HE, (b) AR, (c) LIP LA, (d) LIP BHE, (e) PLIP LA, and (f) PLIP BHE. This shows that PLIP-based algorithms have better results visually.

Fig. 17 shows sample results for one of these images, i.e., cave [Fig. 16(k)]. The resulting images demonstrate the contrast stretching effect by the enhanced algorithms. HE enhances the dark portions of the image shown in Fig. 17(a). However, the image is unnaturally bright. AR enhances the bright portions of the image shown in Fig. 17(b). Nevertheless, many of the details in the darker background are difficult to see.

The LIP and PLIP LAs give similar results as shown in Fig. 17(c) and (e). They enhance both the dark and bright portions of the image. Their resulting images are visually pleasing in which all details are visible. PLIP LA gives slightly better definition. The output image of LIP BHE in Fig. 17(d) shows improved performance compared to traditional HE. However, the result of PLIP BHE shows all details in the bright foreground and the dark background as shown in Fig. 17(f).

Fig. 18 shows the enhanced results of all 12 test images by HE, AR, LIP LA, and PLIP BHE. The results verify that the PLIP BHE show better enhancement performance for each image.

B. Subjective and Objective Evaluation

Two evaluation methods are used to assess the performance of these enhancement techniques. The first is a subjective evaluation method to visually assess the enhanced images by using the mean opinion score (MOS) recommended by ITU-T [56]. The MOS intends to determine which are most visually pleasing for a human observer. The second method uses the EMEE measure as an objective evaluation tool.

In the subjective evaluation, nine human interpreters visually evaluated all enhanced results of 12 images. Each image was given a MOS score of 1–5, where a score of five indicates the best quality. The results in Table III are the average value of the scores given by all human interpreters.

The average score at the bottom of Table III for each enhancement algorithm shows that PLIP BHE, on average, yields more visually appealing enhanced images. This subjective evaluation shows that PLIP BHE outperforms the other algorithms.

However, it is necessary to use an objective criterion as well. All enhanced images are then measured by the EMEE measure individually. The EMEE results are given in Table IV. The high EMEE values of PLIP BHE for each image and the average EMEE values for each enhancement algorithm demonstrate that PLIP BHE outperforms all other algorithms in this study.

It is also appropriate to comment on the robustness of PLIP BHE. Many images are consistently difficult to enhance such as the cell phone images and the copter image. However, they were rated highly by our subjective evaluation when enhanced by PLIP BHE. These images show great improvements when assessed using the EMEE measure. This demonstrates that the proposed PLIP-based algorithms are useful for difficult cases in image enhancement.

In summary, the presented PLIP BHE outperforms the other enhancement methods according to the subjective and objective analysis. Particularly for difficult-to-enhance images such as the cave and copter images, the proposed PLIP BHE provides better visually pleasing results. Moreover, the consistent performance on all images is important for an enhancement algorithm. This further demonstrates the performance of the proposed PLIP BHE. The differences between traditional LIP and PLIP methods are summarized in Table V.

VIII. Conclusion

In this paper, we have introduced a new PLIP model for improving image processing operations such as image fusion

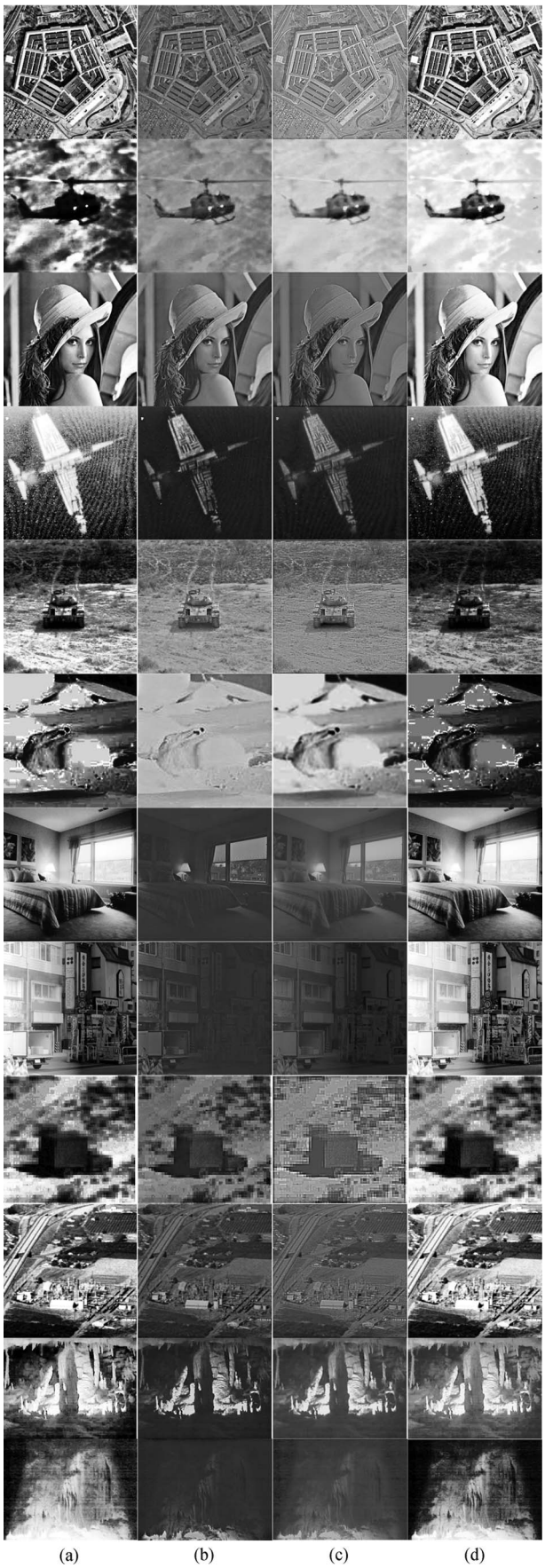

Fig. 18. Enhanced results for all images. (a) HE. (b) AR. (c) LIP LA. (d) PLIP BHE.

TABLE III
SUBJECTIVE EVALUATION OF RESULTS

Image	HE	AR	LA	LIP-LA	LIP-BHE	PLIP-LA	PLIP-AR	PLIP-BHE
Pentagon	3.43	3.43	2.86	2.43	3.29	3.43	3.00	3.43
Copter	1.29	3.71	3.57	2.71	1.57	3.43	4.57	4.14
Lena	3.43	4.14	3.86	3.57	3.71	3.57	1.43	3.43
Plane	2.14	3.29	2.86	1.00	3.00	1.86	3.43	3.14
Tank	2.86	3.29	3.57	2.43	3.29	2.14	2.71	2.00
Arctic Hare	1.71	3.14	3.14	2.86	1.43	3.00	2.43	3.43
Bed	4.14	2.00	2.86	1.71	2.67	1.00	2.57	3.71
Business	4.29	2.57	2.71	2.14	2.57	2.57	3.29	2.43
Truck	2.86	1.86	3.00	1.57	1.29	1.86	3.29	3.29
Plant	4.14	3.57	3.57	2.43	4.14	2.57	3.71	3.71
Cave	3.00	2.86	2.86	2.14	3.43	1.71	3.00	3.57
Rocks	2.57	2.29	2.29	1.57	2.57	1.29	3.14	3.43
Average	**2.99**	**3.01**	**3.10**	**2.21**	**2.75**	**2.37**	**3.05**	**3.31**
1 = Bad, 2 = Poor, 3 = Fair, 4 = Good, 5 = Excellent								

Subjective evaluation results using Mean Opinion Score. The results show that PLIP Bi-Histogram Equalization was deemed more visually pleasing.

TABLE IV
OBJECTIVE EVALUATION OF RESULTS

Image	HE	AR	LA	LIP-LA	LIP-BHE	PLIP-LA	PLIP-AR	PLIP-BHE
Pentagon	0.6090	0.2854	0.3689	0.7731	0.4645	0.7828	0.0283	1.4375
Copter	0.1180	0.0441	0.0402	0.1478	0.1088	0.0587	0.0163	0.1549
Lena	0.5074	0.4360	0.6770	0.4910	0.5137	0.4772	0.0233	0.7512
Plane	1.5016	0.4206	0.4713	2.8852	0.9178	3.3508	0.0103	4.7263
Tank	0.5567	0.3109	0.5079	0.6944	0.6392	1.7488	0.0195	2.8718
Arctic Hare	0.0448	0.0147	0.0144	0.0338	0.0419	0.0229	0.0048	0.0482
Bed	1.1695	2.3665	0.2690	0.8184	9.6555	0.3966	0.0030	3.5204
Business	2.5240	5.2381	4.2662	0.8967	2.0763	1.5420	0.0118	5.3244
Truck	0.9870	2.8184	2.6134	2.3002	1.9627	2.9879	0.0471	3.5437
Plant	1.2986	0.8960	2.0688	2.2296	1.8958	0.9802	0.0361	3.6510
Cave	6.8056	6.4565	5.8500	9.5631	11.085	11.823	0.0222	19.101
Rocks	0.7966	0.3065	0.3084	0.3281	0.5409	0.7304	0.0095	2.2855
Average	**1.4099**	**1.6328**	**1.4546**	**1.7635**	**2.4919**	**2.0751**	**0.0193**	**3.9513**

Objective Evaluation uses EMEE measure. The results show that PLIP Bi-Histogram Equalization outperforms other methods numerically.

and enhancement. By introducing five new parameters μ, γ, k, λ, and β, the new PLIP operations have been shown to provide a more universal and adaptive model that spans from the LIP to linear model and all cases in between. They include the LIP operations when $\mu = \gamma = k = \lambda = M$ and $\beta = 1$, as well as linear arithmetic operations when μ, γ, k, and λ approach the infinity and $\beta = 1$.

Better image fusion performance of the PLIP model has been proven by comparing the PLIP addition with the linear arithmetic and LIP additions. We have demonstrated image fusion properties of the PLIP model: 1) The PLIP addition can yield the intensity image directly from gray-tone images and vice versa; 2) the PLIP multiplication can be used for image fusion, and excellent fusion results can be obtained by choosing appropriate parameter values; and 3) the exponential parameter β has been demonstrated to be able to enhance the image fusion results by the PLIP multiplication.

A training system was presented to help to select these parameters for the PLIP framework. Training the PLIP model parameters was demonstrated by selecting the local extrema from the EMEE versus parameter plots. In addition, we have demonstrated the effectiveness of the trained model for image enhancement in both the spatial and transform domains.

TABLE V
COMPARING THE LIP AND PLIP MODELS BASED ON IMAGING REQUIREMENTS AND APPLICATIONS

Requirements / Applications	Traditional LIP	PLIP
a physically relevant image formation model	Uses gray-tone function	Uses image dependant gray-tone function
Operations must be consistent with physical nature of images	Operations model light absorption filters	Operations model absorption filters with extended range
Operations must be computationally effective	Operations are well-defined and follow important properties	Operations are well-defined and follow important properties
Must be practically fruitful	Demonstrated in [34,37,53,61]	Demonstrated with PLIP Lee's Algorithm, PLIP Bi-Histogram Equalization, and PLIP Alpha Rooting
Minimize the loss of information	Added images are slightly darker than the originals	Processed images are more visually pleasing
Improves on linear arithmetic	Enhanced results are better than linear arithmetic	Enhanced results improve on this using LIP
Relationship between linear arithmetic and logarithmic arithmetic	No	The linear arithmetic is a special PLIP case when the PLIP parameter approaches the infinity
Works for exponentiation	No	PLIP exponentiation is given for PLIP Alpha Rooting
Adapts for different image types or applications	No	PLIP parameters can be fine tuned for different image classes or scenarios using the training methods shown here

We have presented three novel PLIP-based image enhancement algorithms such as PLIP LA, PLIP BHE, and PLIP AR. Computer simulations and comparisons have shown that, by only varying these parameters in the PLIP model, one obtained more visually pleasing results for image enhancement in both the spatial and transform domains to meet human expert approval. Objective image enhancement measures and subjective visual assessments have demonstrated the improvement of the PLIP model for image enhancement. The new PLIP model has potential applications in graphics systems and multimedia processing applications.

APPENDIX

A. Proofs of the PLIP's Property 3 in Section II-B

The PLIP operators revert to linear arithmetic operations when $\gamma(M)$, $k(M)$, and $\lambda(M)$ approach the infinity and $\beta = 1$

$$\lim_{\gamma(M)\to\infty} g_1 \widetilde{\oplus} g_2 = g_1 + g_2 - \lim_{\gamma(M)\to\infty} \frac{g_1 g_2}{\gamma(M)} = g_1 + g_2$$

$$\lim_{k(M)\to\infty} g_1 \widetilde{\Theta} g_2 = \lim_{k(M)\to\infty} k(M) \frac{g_1 - g_2}{k(M) - g_2} = \frac{g_1 - g_2}{1 - \lim_{k(M)\to\infty} \frac{g_2}{k(M)}} = g_1 - g_2$$

$$\lim_{\gamma(M)\to\infty} c \widetilde{\otimes} g = \lim_{\gamma(M)\to\infty} \overbrace{g \widetilde{\oplus} g \widetilde{\oplus} \cdots \widetilde{\oplus} g}^{c} = \overbrace{g + g + \cdots + g}^{c} = cg.$$

If $\beta = 1$, since $\widetilde{\varphi}(g)$ and $\widetilde{\varphi}^{-1}(g)$ are continuous functions

$$\begin{aligned}\lim_{\lambda(M)\to\infty} \widetilde{\varphi}(g) &= \lim_{\lambda(M)\to\infty} \left[-\lambda(M) \ln\left(1 - \frac{g}{\lambda(M)}\right)\right] \\ &= -\lim_{\lambda(M)\to\infty} \frac{\ln\left(1 - \frac{g}{\lambda(M)}\right)}{\frac{1}{\lambda(M)}} \\ &= -\lim_{\lambda(M)\to\infty} \frac{\left[\ln\left(1 - \frac{g}{\lambda(M)}\right)\right]'}{\left[\frac{1}{\lambda(M)}\right]'} \\ &= -\lim_{\lambda(M)\to\infty} \frac{\left(1 - \frac{g}{\lambda(M)}\right)\frac{g}{\lambda^2(M)}}{-\frac{1}{\lambda^2(M)}} = g.\end{aligned}$$

Similarly, $\lim_{\lambda(M)\to\infty} \widetilde{\varphi}^{-1}(g) = g$. Thus

$$\begin{aligned}&\lim_{\lambda(M)\to\infty} \widetilde{\varphi}^{-1}\left(\widetilde{\varphi}(g_1) \cdot \widetilde{\varphi}(g_2)\right) \\ &= \lim_{\lambda(M)\to\infty} \widetilde{\varphi}^{-1}\left(\lim_{\lambda(M)\to\infty} \widetilde{\varphi}(g_1) \lim_{\lambda(M)\to\infty} \widetilde{\varphi}(g_2)\right) \\ &= \lim_{\lambda(M)\to\infty} \widetilde{\varphi}^{-1}(g_1 g_2) = g_1 g_2.\end{aligned}$$

B. Analysis of the Output Range of the PLIP Operations

We first assume that the input gray tone is within $(0, \gamma(M)]$. The PLIP addition can be changed to another format

$$1 - \frac{g_1 \widetilde{\oplus} g_2}{\gamma(M)} = \left[1 - \frac{g_1}{\gamma(M)}\right]\left[1 - \frac{g_2}{\gamma(M)}\right] \geq 0.$$

Thus, the output range of the PLIP addition is $(0, \gamma(M)]$. The PLIP scalar multiplication can also be rewritten as

$$1 - \frac{c \widetilde{\otimes} g}{\gamma(M)} = \left[1 - \frac{g}{\gamma(M)}\right]^c \geq 0.$$

The range of the PLIP scalar multiplication is $(0, \gamma(M)]$.

If the input gray tone is within $(0, k(M)]$, the PLIP subtraction is rewritten as the following format:

$$g_1 \widetilde{\Theta} g_2 = \frac{g_1 - g_2}{1 - \frac{g_2}{k(M)}} = \begin{cases} k(M), & \text{for } g_1 = k(M) \text{ and } g_2 = 0 \\ -\infty, & \text{for } g_2 \to k(M). \end{cases}$$

The range of the PLIP subtraction is $(-\infty, k(M)]$.

ACKNOWLEDGMENT

The authors would like to thank the anonymous reviewers for their valued comments which helped to improve the manuscript. The authors would also like to thank S. Nercessian for his help in mathematically proving the PLIP properties.

REFERENCES

[1] T. G. Stockham, Jr., "Image processing in the context of a visual model," *Proc. IEEE*, vol. 60, no. 7, pp. 828–842, Jul. 1972.
[2] B. Bhanu, J. Peng, T. Huang, and B. Draper, "Introduction to the special issue on learning in computer vision and pattern recognition," *IEEE Trans. Syst., Man, Cybern. B, Cybern.*, vol. 35, no. 3, pp. 391–396, Jun. 2005.
[3] C. Munteanu and A. Rosa, "Gray-scale image enhancement as an automatic process driven by evolution," *IEEE Trans. Syst., Man, Cybern. B, Cybern.*, vol. 34, no. 2, pp. 1292–1298, Apr. 2004.

[4] G. Gilboa, N. Sochen, and Y. Y. Zeevi, "Forward-and-backward diffusion processes for adaptive image enhancement and denoising," *IEEE Trans. Image Process.*, vol. 11, no. 7, pp. 689–703, Jul. 2002.

[5] G. Guidi, J. A. Beraldin, S. Ciofi, and C. Atzeni, "Fusion of range camera and photogrammetry: A systematic procedure for improving 3-D models metric accuracy," *IEEE Trans. Syst., Man, Cybern. B, Cybern.*, vol. 33, no. 4, pp. 667–676, Aug. 2003.

[6] M. W. Powell, S. Sarkar, D. B. Goldgof, and K. Ivanov, "A methodology for extracting objective color from images," *IEEE Trans. Syst., Man, Cybern. B, Cybern.*, vol. 34, no. 5, pp. 1964–1978, Oct. 2004.

[7] S. Y. Chen and Y. F. Li, "Vision sensor planning for 3-D model acquisition," *IEEE Trans. Syst., Man, Cybern. B, Cybern.*, vol. 35, no. 5, pp. 894–904, Oct. 2005.

[8] J. Tang, Q. Sun, and K. Agyepong, "An image enhancement algorithm based on a contrast measure in the wavelet domain for screening mammograms," in *Proc. IEEE Int. Conf. Image Process.*, 2007, pp. V-29–V-32.

[9] K. Huang, Q. Wang, and Z. Wu, "Color image enhancement and evaluation algorithm based on human visual system," in *Proc. IEEE Int. Conf. Acoust., Speech, Signal Process.*, 2004, pp. 721–724.

[10] Y. He, K.-H. Yap, L. Chen, and L.-P. Chau, "A novel hybrid model framework to blind color image deconvolution," *IEEE Trans. Syst., Man, Cybern. A, Syst., Humans*, vol. 38, no. 4, pp. 867–880, Jul. 2008.

[11] L. Guan, "An optimal neuron evolution algorithm for constrained quadratic programming in image restoration," *IEEE Trans. Syst., Man, Cybern. A, Syst., Humans*, vol. 26, no. 4, pp. 513–518, Jul. 1996.

[12] S. K. Naik and C. A. Murthy, "Hue-preserving color image enhancement without gamut problem," *IEEE Trans. Image Process.*, vol. 12, no. 12, pp. 1591–1598, Dec. 2003.

[13] J. Duan and G. Qiu, "Novel histogram processing for colour image enhancement," in *Proc. 3rd Int. Conf. Image Graph.*, 2004, pp. 55–58.

[14] E. Bhattacharya and A.-K. Yan, "Iterative histogram modification of gray images," *IEEE Trans. Syst., Man, Cybern.*, vol. 25, no. 3, pp. 521–523, Mar. 1995.

[15] Y.-T. Kim, "Contrast enhancement using brightness preserving bi-histogram equalization," *IEEE Trans. Consum. Electron.*, vol. 43, no. 1, pp. 1–8, Feb. 1997.

[16] Y. Wang, Q. Chen, and B. Zhang, "Image enhancement based on equal area dualistic sub-image histogram equalization method," *IEEE Trans. Consum. Electron.*, vol. 45, no. 1, pp. 68–75, Feb. 1999.

[17] S.-D. Chen and A. R. Ramli, "Minimum mean brightness error bi-histogram equalization in contrast enhancement," *IEEE Trans. Consum. Electron.*, vol. 49, no. 4, pp. 1310–1319, Nov. 2003.

[18] C. Papaodysseus, M. Exarhos, M. Panagopoulos, P. Rousopoulos, C. Triantafillou, and T. Panagopoulos, "Image and pattern analysis of 1650 B.C. wall paintings and reconstruction," *IEEE Trans. Syst., Man, Cybern. A, Syst., Humans*, vol. 38, no. 4, pp. 958–965, Jul. 2008.

[19] S. Agaian and F. Arslan, "Two transform based image enhancement methods," in *Proc. Int. Signal Process. Conf.*, Dallas, TX, 2003.

[20] G. X. Ritter and J. N. Wilson, "Image algebra in a nutshell," in *Proc. IEEE Int. Conf. Comput. Vis.*, London, U.K., 1987, pp. 641–645.

[21] M. Jourlin and J. Pinoli, "A model for logarithmic image processing," *J. Microsc.*, vol. 149, pp. 21–35, 1988.

[22] J.-C. Pinoli, "The logarithmic image processing model: Connections with human brightness perception and contrast estimators," *J. Math. Imaging Vis.*, vol. 7, no. 4, pp. 341–358, Oct. 1997.

[23] M. Jourlin and J. C. Pinoli, "Logarithmic image processing: The mathematical and physical framework for the representation and processing of transmitted images," *Adv. Imaging Electron Phys.*, vol. 115, pp. 130–196, 2001.

[24] M. Jourlin, J. C. Pinoli, and R. Zeboudj, "Contrast definition and contour detection for logarithmic images," *J. Microsc.*, vol. 156, pp. 33–40, 1989.

[25] M. Jourlin and J.-C. Pinoli, "Image dynamic range enhancement and stabilization in the context of the logarithmic image processing model," *Signal Process.*, vol. 41, no. 2, pp. 225–237, Jan. 1995.

[26] G. Deng, "An entropy interpretation of the logarithmic image processing model with application to contrast enhancement," *IEEE Trans. Image Process.*, vol. 18, no. 5, pp. 1135–1140, May 2009.

[27] G. Deng, L. W. Cahill, and G. R. Tobin, "The study of logarithmic image processing model and its application to image enhancement," *IEEE Trans. Image Process.*, vol. 4, no. 4, pp. 506–512, Apr. 1995.

[28] J.-C. Pinoli, "A general comparative study of the multiplicative homomorphic, log-ratio and logarithmic image processing approaches," *Signal Process.*, vol. 58, no. 1, pp. 11–45, Apr. 1997.

[29] J. Debayle, Y. Gavet, and J.-C. Pinoli, "General adaptive neighborhood image restoration, enhancement and segmentation," in *Image Analysis and Recognition*. Berlin, Germany: Springer-Verlag, 2006, pp. 29–40.

[30] J.-C. Pinoli and J. Debayle, "Logarithmic adaptive neighborhood image processing (LANIP): Introduction, connections to human brightness perception, and application issues," *EURASIP J. Appl. Signal Process.*, vol. 2007, no. 1, p. 114, Jan. 2007.

[31] L. W. Cahill and G. Deng, "An overview of logarithm-based image processing techniques for biomedical applications," in *Proc. 13th Int. Conf. Digital Signal Process.*, 1997, vol. 1, pp. 93–96.

[32] C. Vertan, A. Oprea, C. Florea, and L. Florea, "A pseudo-logarithmic image processing framework for edge detection," in *Proc. Adv. Concepts Intell. Vis. Syst.*, 2008, pp. 637–644.

[33] G. Deng and J.-C. Pinoli, "Differentiation-based edge detection using the logarithmic image processing model," *J. Math. Imaging Vis.*, vol. 8, no. 2, pp. 161–180, Mar. 1998.

[34] J. Debayle and J.-C. Pinoli, "General adaptive neighborhood choquet image filtering," *J. Math. Imaging Vis.*, vol. 35, no. 3, pp. 173–185, Nov. 2009.

[35] J. Debayle and J.-C. Pinoli, "General adaptive neighborhood image processing: Part I: Introduction and theoretical aspects," *J. Math. Imaging Vis.*, vol. 25, no. 2, pp. 245–266, Sep. 2006.

[36] J. Debayle and J.-C. Pinoli, "General adaptive neighborhood image processing: Part II: Practical application examples," *J. Math. Imaging Vis.*, vol. 25, no. 2, pp. 267–284, Sep. 2006.

[37] E. Zaharescu, "Medical Image Enhancement using Logarithmic Image Processing," in *Proc. Int. Conf. Vis., Imaging, Image Process.*, Benidorm, Spain, 2005.

[38] J. M. Palomares, J. Gonzales, E. Ros, and A. Prieto, "General logarithmic image processing convolution," *IEEE Trans. Image Process.*, vol. 15, no. 11, pp. 3602–3608, Nov. 2006.

[39] M. K. Kundu and S. K. Pal, "Thresholding for edge detection using human psychovisual phenomena," *Pattern Recognit. Lett.*, vol. 4, no. 6, pp. 433–441, Dec. 1986.

[40] E. Wharton, S. Agaian, and K. Panetta, "Comparative study of logarithmic enhancement algorithms with performance measure," in *Proc. SPIE—Image Processing: Algorithms and Systems, Neural Networks, and Machine Learning*, San Jose, CA, 2006, p. 606412-12.

[41] S. Agaian, K. Panetta, and A. Grigoryan, "A new measure of image enhancement," in *Proc. Int. Conf. Signal Process. Commun.*, Marbella, Spain, 2000, pp. 19–22.

[42] S. S. Agaian, "Visual morphology," in *Proc. SPIE—Nonlinear Image Processing X*, San Jose, CA, 1999, pp. 139–150.

[43] S. S. Agaian, B. Silver, and K. A. Panetta, "Transform coefficient histogram-based image enhancement algorithms using contrast entropy," *IEEE Trans. Image Process.*, vol. 16, no. 3, pp. 741–758, Mar. 2007.

[44] J. Tang, E. Peli, and S. Acton, "Image enhancement using a contrast measure in the compressed domain," *IEEE Signal Process. Lett.*, vol. 10, no. 10, pp. 289–292, Oct. 2003.

[45] R. Bala, G. Sharma, V. Monga, and J. P. Van de Capelle, "Two-dimensional transforms for device color correction and calibration," *IEEE Trans. Image Process.*, vol. 14, no. 8, pp. 1172–1186, Aug. 2005.

[46] M. Bertalmio, V. Caselles, E. Provenzi, and A. Rizzi, "Perceptual color correction through variational techniques," *IEEE Trans. Image Process.*, vol. 16, no. 4, pp. 1058–1072, Apr. 2007.

[47] M. J. Vrhel and H. J. Trussell, "Filter considerations in color correction," *IEEE Trans. Image Process.*, vol. 3, no. 2, pp. 147–161, Mar. 1994.

[48] J. Tang, J. Kim, and E. Peli, "Image enhancement in the JPEG domain for people with vision impairment," *IEEE Trans. Biomed. Eng.*, vol. 51, no. 11, pp. 2013–2023, Nov. 2004.

[49] Y. Wan and D. Shi, "Joint exact histogram specification and image enhancement through the wavelet transform," *IEEE Trans. Image Process.*, vol. 16, no. 9, pp. 2245–2250, Sep. 2007.

[50] M. Singh, S. Singh, and D. Partridge, "A knowledge-based framework for image enhancement in aviation security," *IEEE Trans. Syst., Man, Cybern. B, Cybern.*, vol. 34, no. 6, pp. 2354–2365, Dec. 2004.

[51] J.-S. Lee, "Digital image enhancement and noise filtering by use of local statistics," *IEEE Trans. Pattern Anal. Mach. Intell.*, vol. PAMI-2, no. 2, pp. 165–168, Mar. 1980.

[52] J. McClellan, "Artifacts in alpha-rooting of images," in *Proc. IEEE Int. Conf. Acoust., Speech, Signal Process.*, 1980, pp. 449–452.

[53] R. G. Kogan, S. S. Agaian, and K. Panetta, "Visualization using rational morphology and zonal magnitude reduction," in *Proc. SPIE—Nonlinear Image Processing IX*, San Jose, CA, 1998, pp. 153–163.

[54] J. K. Kim, J. M. Park, K. S. Song, and H. W. Park, "Adaptive mammographic image enhancement using first derivative and local statistics," *IEEE Trans. Med. Imag.*, vol. 16, no. 5, pp. 495–502, Oct. 1997.

[55] S. Aghagolzadeh and O. K. Ersoy, "Transform image enhancement," *Opt. Eng.*, vol. 31, no. 3, pp. 614–626, Mar. 1992.

[56] Methods for Subjective Determination of Transmission Quality, ITU-T Recommendation P.800, 1996.

Karen Panetta (S'84–M'85–SM'95–F'08) received the B.S. degree in computer engineering from Boston University, Boston, MA, and the M.S. and Ph.D. degrees in electrical engineering from Northeastern University, Boston.

She is currently a Professor of electrical and computer engineering with Tufts University, Medford, MA, and the Founder of the Nerd Girls Program to promote women in engineering. She is also a Consulting Engineer with Tyco Electronics Inc., Lowell, MA. She is a Cofounder of BA Logix, Inc., Quincy, MA, and serves as the company's Chief Research Scientist. She is the 2007–2009 IEEE Director of Women in Engineering and the Editor-in-Chief of the *IEEE Women in Engineering Magazine*.

Sos Agaian (M'98–SM'00) received the M.S. degree (*summa cum laude*) in mathematics and mechanics from Yerevan State University, Yerevan, Armenia, the Ph.D. degree in mathematics and physics and the Doctor of Engineering Sciences (equivalent to the U.S. Doctor degree in electrical and computer engineering) degree from the Academy of Sciences of the USSR, Moscow, Russia, and the Diploma in computer science (equivalent to the U.S. Ph.D. degree in computer science) from the Supreme Attestation Board of the USSR, Moscow.

He is currently the Peter T. Flawn Distinguished Professor with the College of Engineering, The University of Texas, San Antonio, and an Adjunct Professor with the Department of Electrical and Computer Engineering, Tufts University, Medford, MA. He is an Associate Editor of the *Journal of Real-Time Imaging* and the *Journal of Electronic Imaging* and an Editorial Board Member of the *Journal of Pattern Recognition and Image Analysis*. He has authored more than 370 scientific papers and 4 books and is the holder of 13 patents. His current research interests lie in the broad area of signal/image processing and transmission, information security, and mobile imaging and secure communication.

Dr. Agaian is a fellow of the Society of Photo-Optical Instrumentation Engineers.

Yicong Zhou (M'07) received the B.S. degree in electrical engineering from Hunan University, Changsha, China, and the M.S. degree in electrical engineering from Tufts University, Medford, MA, where he is currently working toward the Ph.D. degree in electrical engineering.

His current research interests include multimedia security, image enhancement, medical imaging, and signal/image processing.

Mr. Zhou is a member of the Society of Photo-Optical Instrumentation Engineers.

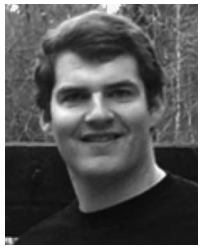

Eric J. Wharton (S'04) received the B.S. degree in electrical engineering from Tufts University, Medford, MA, where he is currently working toward the M.S. degree.

His primary research interests include digital signal and image processing, specifically image enhancement and performance measures.

Mr. Wharton is a member of Eta Kappa Nu and Tau Beta Pi.